

# Characteristics of adsorbed CO and CH<sub>3</sub>OH oxidation reactions for complex Pt/Ru catalyst systems

C. Bock\*, M.-A. Blakely, B. MacDougall

*National Research Council Canada, Montreal Road, Ottawa, Ont., Canada K1A 0R6*

Received 22 July 2004; received in revised form 14 September 2004; accepted 11 October 2004

Available online 21 November 2004

## Abstract

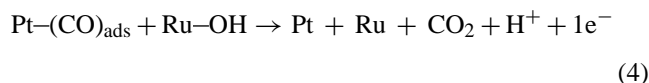
Pt/Ru powder catalysts of the same nominal Pt to Ru composition were prepared using a range of methods resulting in different catalyst properties. Two PtRu alloy catalysts were prepared, one of which has essentially the same surface and bulk Pt to Ru composition, while the second catalyst is surface enriched with Ru. Two powders consisting of non-alloyed Pt phases and surfaces enriched with Ru were also prepared. The oxidation state of the surface Ru of the latter two catalysts is mainly metallic Ru or Ru-oxides. The catalyst consisting of Ru-oxides was formed at 500 °C. Part of this catalyst was then reduced in a H<sub>2</sub> atmosphere under “mild” conditions, thus catalyst properties such as particle size are not changed, as they are locked in during previous high temperature treatment. The oxidation kinetics of adsorbed CO (CO<sub>ads</sub>) and solution CH<sub>3</sub>OH were studied and compared to the Ru ad-metal state and Pt to Ru site distribution of the as-prepared catalysts. The kinetics of the CO<sub>ads</sub> oxidation reaction were observed to be slower for the catalyst containing Ru-oxides as opposed to mainly Ru metal. The CH<sub>3</sub>OH oxidation activities measured per Pt surface area, i.e., the catalytic activities are better (by ca. seven times) for the alloy catalysts than the non-alloyed Pt/Ru catalysts. The latter two catalysts showed essentially the same catalytic CH<sub>3</sub>OH oxidation activities, i.e., independent of the Ru ad-metal oxidation state of the as-prepared catalysts. Furthermore, it is shown that CO<sub>ads</sub> oxidation experiments can be used to extract characteristics that allow the comparison of catalytic activities for the CO<sub>ads</sub> oxidation reaction and Pt to Ru site distribution for complex catalyst systems.

Crown Copyright © 2004 Published by Elsevier Ltd. All rights reserved.

*Keywords:* Fuel cells; Platinum; Ruthenium; Carbon monoxide; Methanol

## 1. Introduction

Direct methanol and reformate fuel cells are emerging as potential power sources for portable devices and transportation purposes. Among other obstacles, the performance of the anode catalysts towards the oxidation of methanol and/or CO to CO<sub>2</sub> needs to be improved. Pt/Ru catalysts have shown superior performance for the CH<sub>3</sub>OH and CO oxidation reactions [1,2]. The beneficial catalytic effect has been attributed to a bi-functional mechanism, as shown in the following scheme for the case of the CH<sub>3</sub>OH oxidation reaction [2]:



As a result of the adsorption/dehydrogenation reaction of CH<sub>3</sub>OH that takes place on Pt sites, an intermediate “CO”-type species is formed. This species is believed to be oxidized to CO<sub>2</sub> with the assistance of –OH species, which are formed by the partial oxidation of H<sub>2</sub>O on Ru surface sites. Based on this reaction scheme, it is clear that the ratio and distribution of Pt and Ru catalyst surface sites influences the CH<sub>3</sub>OH oxidation kinetics [3–5]. In fact, prior work has shown that catalysts consisting of homogeneously distributed surface sites

\* Corresponding author. Tel.: +1 613 990 2252; fax: +1 613 941 2529.  
E-mail address: [christina.bock@nrc-cnrc.ca](mailto:christina.bock@nrc-cnrc.ca) (C. Bock).

of 70–30 atomic percent (at.%) Pt to Ru ratio display the best activity for the CH<sub>3</sub>OH oxidation reaction [5]. The chemical state of the Ru ad-metal component has also been suggested to influence the CH<sub>3</sub>OH oxidation kinetics significantly [6]; however, there is disagreement regarding the most active form of Ru. Bimetallic PtRu alloy catalysts have been reported to show significantly poorer (ca. 250 times lower) activities for the CH<sub>3</sub>OH oxidation reaction than catalysts consisting of mixtures of Pt metal and various Ru-oxides [7]. Based on these results, it was recommended that PtRu alloys should not be used as catalysts for direct methanol fuel cells [6]. In subsequent studies [7,8], it was suggested that Ru in its metallic state is most active for the CH<sub>3</sub>OH oxidation reaction. The authors of the first study [7] used commercially available unsupported partially alloyed Pt/Ru catalysts. They based their conclusions mainly on adsorbed CO (CO<sub>ads</sub>) to CO<sub>2</sub> oxidation studies for the as-received and H<sub>2</sub> reduced catalysts, i.e., involving a limited number of catalysts. In the second study [8], XPS was used to obtain the chemical state of the Ru immediately before and after CH<sub>3</sub>OH oxidation studies were carried out using Pt/Ru and Pt/Ru-oxide catalysts. This study showed that Ru-oxides including RuO<sub>2</sub> are at least partially reduced to metallic Ru in the electrochemical environment; a result supported by another report [9]. Other papers also addressed the issue of the influence of the Ru ad-metal state of the as-prepared catalysts [10,11]. Different Pt/Ru-oxide catalysts were formed within a broad and high temperature range between 400 and 600 °C [10], while in another study an unsupported PtRu alloy catalyst [11] was heat-treated at various temperatures (up to 200 °C) and atmospheres to achieve different oxidation states of the Ru ad-metal of the as-prepared catalysts. Unfortunately, treating and preparing Pt/Ru catalysts at high temperatures typically alters a number of properties such as alloy composition, Pt to Ru surface distribution, particle size as well as oxidation state [5], thus making it difficult to correlate catalytic activities with a particular catalyst property.

In the present investigation, the influence of the ad-metal state of the Ru of the as-prepared catalysts on the oxidation reactions of CO<sub>ads</sub> and CH<sub>3</sub>OH is investigated using four Pt/Ru powder catalysts. The influence of the Pt to Ru surface site distribution on these reactions is also discussed. The Pt/Ru powders are prepared so that different Ru oxidation states and Pt to Ru surface site distributions are obtained. All powder catalysts are characterized using X-ray diffraction (XRD), X-ray photon spectroscopy (XPS), energy diffraction spectroscopy (EDX) and field emission scanning electron microscopy (FESEM). Both the CH<sub>3</sub>OH and CO<sub>ads</sub> oxidation kinetics are studied. Kinetic studies of the CO<sub>ads</sub> oxidation reaction are carried out at low potentials where the –OH nucleation rate on Pt versus the –OH nucleation rate on Ru sites is small. The CO<sub>ads</sub> oxidation data are used to distinguish the different catalysts with regard to their abilities such as –OH nucleation site formation as well as to gain insight into the CO<sub>ads</sub> diffusion distance. The CO<sub>ads</sub> oxidation data are also compared to the true catalytic activity, i.e., oxidation current

per Pt area of the individual catalysts toward the CH<sub>3</sub>OH oxidation reaction.

## 2. Experimental

### 2.1. Catalyst powder preparation

Unsupported Pt and Pt/Ru powders were prepared for this study. The latter consisted of bulk Pt to Ru ratios of 70–30 at.% that is equivalent to the optimal alloy ratio for the CH<sub>3</sub>OH oxidation reaction [5]. The catalysts were prepared, as follows: the Pt powder was prepared by reducing 2.03 g of PtCl<sub>4</sub> (99.9% purity, Alfa & Aesar) dissolved in 150 mL of H<sub>2</sub>O with 75 mL of 0.2 M NaBH<sub>4</sub> (Anachemia); a PtRu alloy was formed by the simultaneous and rapid reduction [5] of 2.6767 g PtCl<sub>4</sub> and 0.5603 g RuCl<sub>3</sub> (99.99% purity, Alfa & Aesar) dissolved in 150 mL of H<sub>2</sub>O with 75 mL of 0.2 M NaBH<sub>4</sub>. This catalyst powder is referred to as PtRu (chemically reduced); a Pt/RuO<sub>2</sub> (thermal) catalyst was formed by mixing (using a mortar) 1.55 g of the Pt powder with 0.5603 g of RuCl<sub>3</sub>. The RuCl<sub>3</sub> was subsequently decomposed in air at 500 °C; a Pt/Ru (H<sub>2</sub> reduced) catalyst was formed by reducing the Pt/RuO<sub>2</sub> (thermal) catalyst at 100 °C in a H<sub>2</sub> atmosphere for 1 h; a Pt/RuO<sub>2</sub> (ball-mill) catalyst was formed by ball-milling 2.83 g Pt powder (–200 mesh, 99.98%, Alfa & Aesar) and 0.85 g RuO<sub>2</sub> (Electronic Grade, Premion, 99.95%, Alfa & Aesar) using a Spex2000 ball mill mixer for 40 h. Three grams of Al powder (–40 + 325 mesh, 99.8%, Alfa & Aesar) and 0.2 g of NaF (Anachemia) were also added to the mixture following a procedure described elsewhere [12]. The powders were mixed in a tungsten carbide (WC) container (50 cm<sup>3</sup>, Spex) with four WC balls (each ball with diameter of 7/16 in., Spex). The ball-milled powder mixture was leached in 1000 mL of 1 M NaOH (EM Science, Merck, ACS grade) solution for 20 h to dissolve the aluminum. After preparation, the Pt and Pt/Ru powder catalysts were washed excessively with H<sub>2</sub>O, filtered and dried in an air oven at 80 °C. The PtCl<sub>4</sub> and RuCl<sub>3</sub> precursor salts were dried in an air oven at 135 °C prior to their use.

### 2.2. Working electrode preparation

The catalyst powders were formed into electrodes by sonicating 13 mg of a particular powder dispersed in solutions consisting of 300 µL of a Nafion<sup>®</sup>117 solution (5 wt.% Nafion dissolved in lower alcohols, Fluka) and 2 mL of H<sub>2</sub>O for 30 min. Appropriate amounts (1–20 µL) of the suspensions were pipetted onto ca. geometrical area of 0.35 cm<sup>2</sup> Au foil electrodes (99.9% Au, 0.1 mm thick, Goodfellow) forming thin catalyst layers. The electrodes were dried in air and room temperature. The Au foils were firmly attached to Au wire electrodes and Au not covered with the catalyst powder was carefully wrapped with Teflon tape.

### 2.3. Cells and electrodes

Three compartment cells, in which the reference electrode was separated from the working and counter electrode compartment by a Luggin capillary, were employed for the electrochemical studies. All potentials reported in this paper are versus the reversible hydrogen electrode (RHE), even though either a mercury sulfate electrode (MSE = −0.68 V versus RHE [13]) or a saturated calomel electrode (SCE = −0.24 V versus RHE [13]) were used for the actual experiments. A large surface area Pt gauze served as counter electrode.

### 2.4. Techniques and instrumentations

Electrochemical experiments were performed using Solartron SI 1287 electrochemical interface (Solartron Group Ltd.) driven by Corrware software program (Scribner, Assoc.). A Scintag XDS2000 system was employed using a Cu K $\alpha$  source to obtain XRD spectra of the catalysts. The scanning angle  $2\theta$  extended from 20° to 80°. The software program Topas 2 (DIFFRAC<sup>PLUS</sup> Topas, Bruker axis Inc.) was employed to extract lattice parameter constants from the experimental XRD spectra. The entire XRD spectra from 20° to 80° were employed to analyse the data. Si powder (typically 1–20  $\mu\text{m}$ , 99.9985% purity, Alfa & Aesar) was used as internal standard for the XRD analysis. XPS spectra were obtained using a Kratos Axis Ultra spectrometer equipped with a monochromatized Al K $\alpha$  source. The catalyst powders were attached to sticky Cu tape (3M copper tape, Soquelec, Montreal) for the XPS analyses. For each catalyst, a survey spectrum was collected before high-resolution spectra of the C 1s, O 1s, Pt 4f, Ru 3p and Ru 3d core level regions were collected. Deconvolutions of the XPS spectra were performed using a CasaXPS Version 2.1.34 (Neal Fairley). A Hitachi S-4800 SEM and EDX were also employed. The XRD, XPS and Field emission scanning electron microscopy characterizations were carried out on the unused, i.e., as-prepared catalyst powders.

### 2.5. CO adsorption ( $CO_{ads}$ )

CO was adsorbed onto the Pt based powder electrodes at 0.15 V by bubbling CO gas (Matheson purity, Matheson gas) through the 0.5 M H<sub>2</sub>SO<sub>4</sub> solution for 20 min. Solution CO was subsequently removed by bubbling high purity Argon gas (Air Products) for 30 min holding the potential at 0.15 V. The potential was then either cycled starting at 0.15 V for two complete oxidation/reduction cycles or stepped to a particular potential value, as mentioned in the appropriate section of the text.

### 2.6. Solutions

All CH<sub>3</sub>OH oxidation studies were carried out using 0.5 M CH<sub>3</sub>OH + 0.5 M H<sub>2</sub>SO<sub>4</sub> solutions. Prior to the electrochemi-

cal studies, the solutions were deoxygenated using high purity Argon gas. ACS grade chemicals and high resistivity 18 M $\Omega$  water were used. The experiments were carried out at room temperature.

## 3. Results and discussion

### 3.1. Characterization of the as-prepared Pt and Pt/Ru catalysts

#### 3.1.1. XRD characterization

Fig. 1 shows raw XRD spectra for the Pt based powders prepared in this work. In all spectra, the diffraction peaks of Si that was homogeneously mixed with the Pt/Ru powders and used as internal standard are clearly recognizable. The entire spectra were used to obtain lattice parameter values for the various phases as well as microstrain and particle size estimations using the Topas software program. The data are shown in Table 1. The following space groups were used for the XRD data fitting: Pt: Fm-3m(225), Ru: P63/mmc(194) RuO<sub>2</sub>: P4<sub>2</sub>/mnm(136) and Al<sub>2</sub>O<sub>3</sub>: R-3c(167) [14]. In the case of PtRu alloy formation, the lattice parameter values estimated for the fcc Pt phase ( $a_{\text{Pt(fcc)}}$ ) in nanometers were used to calculate the amount of Ru dissolved in the Pt lattice using a Vegard's law relationship of:

$$\text{Pt (at. \%)} = \frac{a_{\text{Pt(fcc)}} - 0.3778}{1.5 \times 10^{-4}} \quad (5)$$

This relationship has been determined in previous work based on ab-initio calculations as well as on experimental data [5].

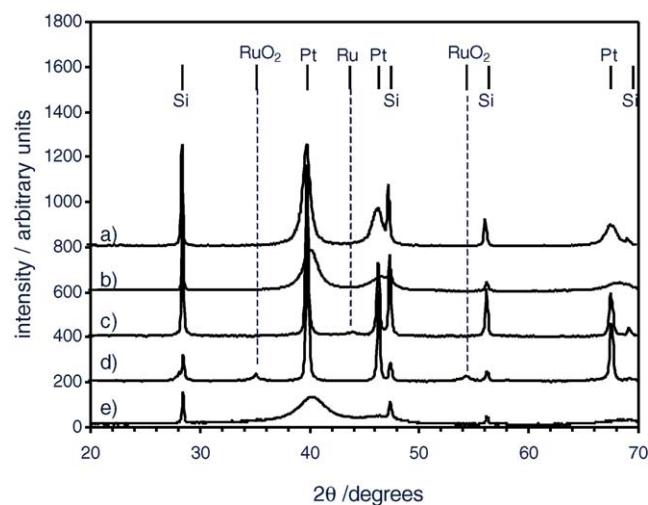


Fig. 1. Slow scan XRD data for Pt and Pt/Ru powders as follows: (a) Pt, (b) PtRu (chemically reduced), (c) Pt/Ru (H<sub>2</sub> reduced), (d) Pt/RuO<sub>2</sub> (thermal) and (e) Pt/RuO<sub>2</sub> (ball-mill) powder. Silicon powder was homogeneously mixed with the catalyst powders as internal standard. XRD spectra were obtained between  $2\theta$ 's of 20° and 80° using a step size of 0.06° and an acquisition time of 60 s.

Table 1  
XRD characteristics for the as-prepared Pt and Pt/Ru catalyst powders<sup>a</sup>

Catalyst	Phase	$a_{\text{Pt(fcc)}}^b$ (nm)	Crystallite size <sup>b</sup> (nm)	Micro-strain <sup>b</sup> (%)	Comments
Pt	Pt fcc	$0.39231 \pm 6 \times 10^{-5}$	$25 \pm 1$	$1 \pm 5 \times 10^{-2}$	1 phase: Pt fcc (100 at.% Pt)
PtRu (chemically reduced)	Pt fcc	$0.3886 \pm 1 \times 10^{-5}$	$14 \pm 1.5$	$2.5 \pm 1.7 \times 10^{-1}$	1 phase: PtRu alloy (70:30 at.% Pt:Ru ratio)
Pt/RuO <sub>2</sub> (thermal)	Pt fcc	$0.3923 \pm 3 \times 10^{-4}$	$30 \pm 5$	$0.14 \pm 3 \times 10^{-2}$	2 phases: Pt fcc (100 at.% Pt) + RuO <sub>2</sub> phase
	RuO <sub>2</sub> tetragonal	$a: 0.4503 \pm 3 \times 10^{-4}$ $c: 0.3115 \pm 3 \times 10^{-4}$			
Pt/Ru (H <sub>2</sub> reduced)	Pt fcc	$0.39251 \pm 2 \times 10^{-5}$	$30 \pm 5$	$0.3 \pm 3 \times 10^{-2}$	2 phases: Pt fcc (100 at.% Pt) + Ru metal phase
	Ru hexagonal	$a: 0.2698 \pm 4 \times 10^{-4}$ $c: 0.4407 \pm 9 \times 10^{-4}$			
Pt/RuO <sub>2</sub> (ball-mill)	Pt fcc	$0.3883 \pm 1.6 \times 10^{-4}$	$5 \pm 1$	$3.5 \pm 1$	2 phases: PtRu-alloy (70:30 at.% Pt:Ru ratio) and Al-oxide (Al <sub>2</sub> O <sub>3</sub> ) phase
	Al <sub>2</sub> O <sub>3</sub> trigonal	$a: 0.486 \pm 3 \times 10^{-3}$ $c: 1.3 \pm 1.5 \times 10^{-3}$			

<sup>a</sup> All catalysts powders have a nominal Pt to Ru ratio of 70–30 at.%, except for the Pt powder.

<sup>b</sup> Values are estimated from the raw XRD data using the Topas software program.

The diffraction peak characteristics for Platinum are clearly recognizable in the XRD spectra for all Pt based powders. The Pt(1 1 1) peak that is observed at  $2\theta$  values varying between  $39.8^\circ$  and  $40.2^\circ$  (indicating different degrees of PtRu alloy formation) is the highest intensity peak for all catalysts. The diffraction peak for the Pt(1 1 1) phase for the Pt powder catalyst is located at a  $2\theta$  value of  $\sim 39.8^\circ$ . For this catalyst, an  $a_{\text{Pt(fcc)}}$  value of  $0.39231 (\pm 6 \times 10^{-5})$  nm is estimated, consistent with data typically observed for Pt [12]. For both the Pt/Ru (H<sub>2</sub> reduced) and the Pt/RuO<sub>2</sub> (thermal) powders, the positions of the Pt(1 1 1) diffraction peak, and hence also the  $a_{\text{Pt(fcc)}}$  values are essentially the same as for the Pt only catalyst (see Table 1). These results indicate that these two powders consist of Pt that is present as a non-alloyed phase. In the case of the Pt/RuO<sub>2</sub> (thermal) powder, diffraction peaks assigned to rutile RuO<sub>2</sub> are observed at  $2\theta$  values of  $\sim 35.2^\circ$  and  $\sim 54.4^\circ$  [14] while for the Pt/Ru (H<sub>2</sub> reduced) powder, a diffraction peak typical for hexagonal Ru(1 0 1) is observed at a  $2\theta$  value of  $\sim 44^\circ$  [14]. In the case of the PtRu (chemically reduced) powder, the position of the Pt(1 1 1) diffraction peak is shifted to a higher  $2\theta$  value of  $\sim 40.2^\circ$ . For this powder, an  $a_{\text{Pt(fcc)}}$  value of  $0.3886 (\pm 1 \times 10^{-5})$  nm was estimated that suggests that close to 30 at.% of Ru is dissolved in the Pt fcc lattice. The fitting of the XRD raw data for this powder only required the Pt fcc phase, i.e., the addition of a Ru phase was not needed, thus being consistent with the view that Ru is completely dissolved in the Pt fcc lattice. The XRD spectra for the Pt/RuO<sub>2</sub> (ball-mill) powder shows that the Pt(1 1 1) diffraction peak is also shifted to a higher  $2\theta$  value of  $\sim 40.2^\circ$ . Essentially the same  $a_{\text{Pt(fcc)}}$  lattice parameter value of  $0.3883 (\pm 1.6 \times 10^{-4})$  nm was estimated for the ball-mill catalyst as for the PtRu (chemically reduced) powder indicating that a PtRu alloy of 70–30 at.% Pt to Ru is formed for the two catalysts. For the analysis of the XRD data of the ball-milled catalyst, a Pt fcc phase was used. It was also necessary to in-

clude a second trigonal Al<sub>2</sub>O<sub>3</sub> phase to obtain a good fit. The presence of Al in the ball-mill catalyst powder was confirmed by XPS and EDX analyses (see below). This indicates that leaching in NaOH is insufficient to completely leach the Al from this catalyst consistent with previous reports [12].

Table 1 also lists the crystallite size values estimated from the Pt diffraction peaks using the Topas software program for the five catalysts prepared in this work. The XRD data suggest that the crystallite sizes for the catalyst powders used in this work are different depending on the preparation method used as expected. It is noteworthy that the XRD data suggest the crystallite size of the Pt/RuO<sub>2</sub> (thermal) and the Pt/Ru (H<sub>2</sub> reduced) catalysts to essentially be the same. This indicates that the reduction of the Pt/RuO<sub>2</sub> (thermal) catalyst in the H<sub>2</sub> atmosphere at the moderate temperature of  $100^\circ\text{C}$  did not affect the crystallite size of these two catalysts. This result is not surprising, as the Pt/RuO<sub>2</sub> (thermal) catalyst was prepared at  $500^\circ\text{C}$ , thus locking in physical properties such as crystallite and particle size (the latter will be discussed using FESEM images). Therefore, it appears reasonable to assume that the reduction of the surface oxides are the sole changes introduced by the low temperature H<sub>2</sub> treatment.

### 3.1.2. XPS characterization

Table 2 summarizes the XPS characteristics of the unused Pt and Pt/Ru powder catalysts. The Pt to Ru (at.%) ratios were also obtained from the XPS data. The mean free path values for Pt 4f and Ru 3p are very similar, namely 1.684 and 1.536 nm, respectively [15]. Therefore, the XPS data reflect the surface Pt to Ru ratios in the case of particles of uniform Pt to Ru distribution. In the case of powders of catalyst particles consisting of non-uniform Pt and Ru concentrations, the Pt to Ru ratios determined from XPS data may not present a true measurement of the Pt to Ru surface ratios. This is likely to the case, for Pt particles having surfaces enriched

Table 2  
XPS characteristics for the as-prepared Pt and Pt/Ru catalyst powders

Catalyst	Species	Assignment	Binding energy <sup>a</sup> (eV)	at.% Pt:Ru ratio <sup>b</sup>	at.% per species <sup>c</sup>
PtRu (chemically reduced)	Pt 4f <sub>7/2</sub>	Pt metal	71.3	70:30	52
		PtO	72.2		19
		Pt-chlorides	74.1		29
	Ru 3p <sub>3/2</sub>	Ru metal	462		69
		Intermediate between Ru metal and RuO <sub>2</sub>	465.1		31
Pt/RuO <sub>2</sub> (thermal)	Pt 4f <sub>7/2</sub>	Pt metal	71.2	36:64	45
		PtO	72.4		10
		PtO <sub>2</sub>	74.2		45
	Ru 3p <sub>3/2</sub>	Intermediate between Ru metal and RuO <sub>2</sub>	462.8		75
		RuO <sub>2</sub>	466		25
Pt/Ru (H <sub>2</sub> reduced)	Pt 4f <sub>7/2</sub>	Pt metal	71.3	44:56	74
		PtO	72.2		26
		PtO <sub>2</sub>	74.3		18
	Ru 3p <sub>3/2</sub>	Ru metal	462		69
		Intermediate between Ru metal and RuO <sub>2</sub>	463.5		31
Pt/RuO <sub>2</sub> (ball-milled)	Pt 4f <sub>7/2</sub>	Pt metal	71.3	54:46	58
		PtO	72.6		24
		PtO <sub>2</sub>	74.3		18
	Ru 3p <sub>3/2</sub>	Ru metal	462		65
		Intermediate between Ru metal and RuO <sub>2</sub>	465		35

<sup>a</sup> The binding energy values were corrected for possible charging effects using the C 1s peak at 284.4 V [13].

<sup>b</sup> At.% Pt to Ru ratio were estimated from the raw XPS signals of the Pt 4f and Ru 3p peaks using sensitivity factors of 5.575 and 2.043, respectively.

<sup>c</sup> At.% ratio calculated for a particular species, i.e., Pt or Ru.

with Ru. The XPS data for the PtRu (chemically reduced) catalyst have been discussed in previous work [5]. The fact that in the case of this particular powder, the Pt to Ru ratio estimated from the XPS data is the same as the Pt to Ru bulk alloy ratio determined from the XRD data suggest that catalyst particles of uniform Pt and Ru concentrations are formed. This has been further supported by CO<sub>ads</sub> stripping voltametric experiments [5], which are essentially the same as found for well characterized bulk metal PtRu alloys of 70–30 at.% Pt to Ru surface ratio. In the case of the Pt/RuO<sub>2</sub> (thermal) and the Pt/Ru (H<sub>2</sub> reduced) powders, the Pt to Ru atomic ratio are clearly different from the nominal 70 to 30 at.% ratio. It is likely that the Pt to Ru atomic ratios determined from the XPS data do not reflect the exact surface composition for these two catalyst powders. The XPS data suggest that the surfaces of these two catalysts are enriched with Ru. This appears reasonable as the method used to prepare these powders (impregnating Pt powders with the RuCl<sub>3</sub> precursor salt) is expected to result in catalyst powders of non-uniform Pt to Ru composition with Ru preferably located on the preformed Pt particle surface. The Pt to Ru atomic ratios estimated from the XPS data of the Pt/RuO<sub>2</sub> (ball-mill) catalyst are also different from their nominal ratio, thus indicating that the Pt and Ru components are not uniformly distributed for this catalyst. However, in the case of the latter, the ball-milling is believed to improve the distribution between the Pt to Ru sites. Furthermore, the XPS data also indicated the presence of Al (ca. 30 at.% Al per Pt + Ru + Al) on this catalyst surface.

The binding energy values and the correspondingly assigned species of the deconvoluted Pt 4f and Ru 3p core level regions of the catalysts studied in this work are also shown in Table 2. Small amounts of Pt-chlorides are found for the PtRu (chemically reduced) catalyst. It should be noted that the Pt-chlorides are believed to be located on the catalyst surface. The actual amount of chlorides per catalyst weight is expected to be very small, as Pt-chlorides were not detected in the XRD and EDX spectra that reflect the bulk catalyst properties. The XPS data for the Pt 4f region for the Pt and Pt/Ru powders suggest Pt to be present as both Pt metal and PtO. However, PtO<sub>2</sub> is also detected for the Pt/RuO<sub>2</sub> (thermal) powder. This is expected, as this catalyst was heat-treated at 500 °C in air, thus resulting in the oxidation of the catalyst surface. It should be noted that neither PtO nor PtO<sub>2</sub> phases are observed in the XRD spectra of the Pt/RuO<sub>2</sub> (thermal) powder, i.e., the XRD data suggest the presence of only a metallic Pt phase for this powder. Therefore, it is believed that only the Pt surface is being oxidized to PtO and PtO<sub>2</sub>. Furthermore, the electrochemical characteristics, namely the cyclic voltamograms for a Pt powder heat-treated at 500 °C in O<sub>2</sub> for 1 h were the same as for polycrystalline Pt metal, suggesting that the Pt-oxides are easily reduced electrochemically. The data for the Ru 3p core level region show that the form of Ru present on the catalyst surfaces depends on the preparation procedure. The Ru on the surfaces for the PtRu (chemically reduced), the Pt/Ru (H<sub>2</sub> reduced) and the Pt/RuO<sub>2</sub> (ball-mill) catalysts is suggested to be mainly Ru metal (between 60 and 80%) and an intermediate form

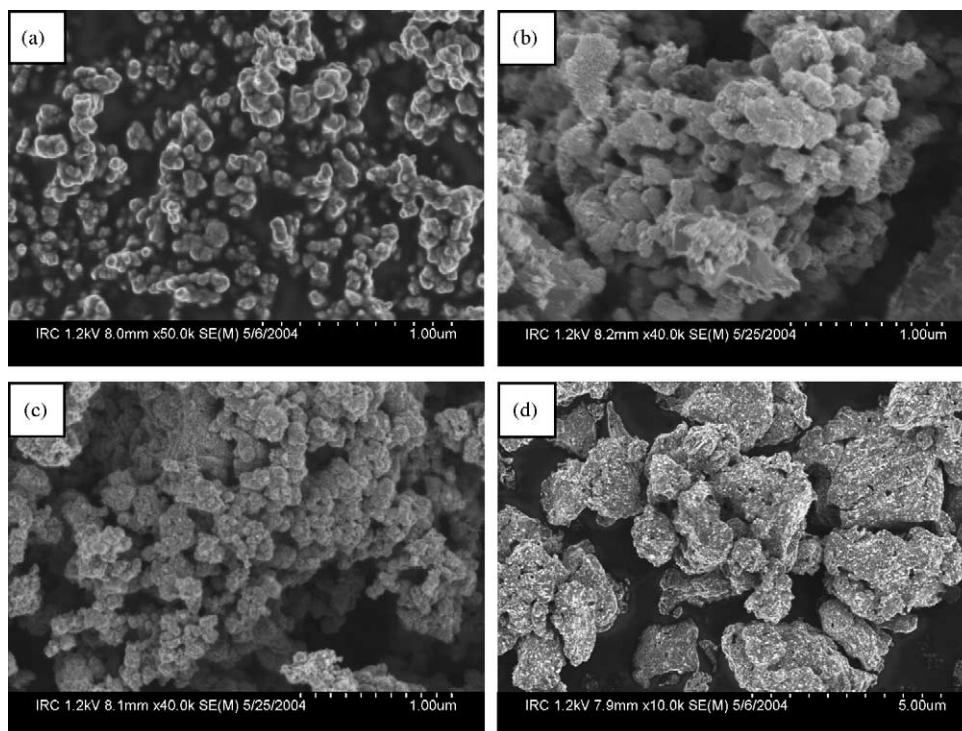


Fig. 2. FESEM images for (a) PtRu (chemically reduced) catalyst powder at a 50,000 $\times$  magnification, (b) Pt/RuO<sub>2</sub> (thermal) catalyst powder at a 40,000 $\times$  magnification, (c) Pt/Ru (H<sub>2</sub> reduced) catalyst at a 40,000 $\times$  magnification and (d) Pt/RuO<sub>2</sub> (ball-mill) catalyst at a 10,000 $\times$  magnification.

between the metallic and (+IV)-state (between 40 and 20%). The XPS data for the Pt/RuO<sub>2</sub> (thermal) catalyst suggest that the Ru on the catalyst surface is present in its oxidized forms, ca. 25% in the +IV state, i.e., as RuO<sub>2</sub> and ca. 75% in its intermediate form between the metallic and (+IV)-state. The XPS data (consistent with the XRD results) strongly suggest that the Ru-oxide powder is reduced to mainly Ru metal during ball-milling. Ball-milling is a high energy process carried out in an inert atmosphere and in the presence of Al that could be oxidized to Al-oxide, while the Ru-oxides are reduced. It has been reported that Mo-oxides are reduced to Mo metal during ball-milling [16]. It is noteworthy that small amounts of chlorides were found for Pt/RuO<sub>2</sub> (thermal) catalysts that were analyzed immediately after preparation, i.e., were not washed with H<sub>2</sub>O. Chlorides were not detected by XPS analysis carried out for well-rinsed (with H<sub>2</sub>O) Pt/RuO<sub>2</sub> (thermal) catalysts indicating that these water-soluble chlorides are removed. This is consistent with previous reports for thermally prepared Pt/RuO<sub>2</sub> [10] and RuO<sub>2</sub> [17] electrodes.

### 3.1.3. FESEM and EDX characteristics

Fig. 2a–d show FESEM images for the alloy, thermal, H<sub>2</sub> reduced and ball-milled Pt/Ru catalysts, respectively. The PtRu catalyst (Fig. 2a) produced by the rapid chemical reduction method is seen to consist of well-ordered particles in the nano-scale range (varying between ca. 20 and 120 nm in diameter). Larger clumps of particles are recognizable that seem to have been formed by growing from inside out. The

catalyst morphology observed by FESEM for the thermal and H<sub>2</sub> reduced powders are seen to be essentially the same (Fig. 2b and c). This is consistent with the view that reduction in the H<sub>2</sub> atmosphere at the moderate temperature of 100 °C results in mainly the reduction of the surface oxides that were formed at 500 °C. In both cases, the catalysts consist of individual particles in the 30 to 160 nm size range, i.e., showing a slightly broader particle size distribution than the PtRu (chemically reduced) catalyst. The surfaces of the individual particles for the H<sub>2</sub> reduced and the thermal catalysts are also rougher than seen for the PtRu catalyst formed by chemical reduction. Furthermore, the particles appear to be fused together rather than grown from inside out as seen for the PtRu (chemically reduced) catalyst reflecting the differences in the preparation methods. In contrast to the first three catalysts, the morphology of the ball-mill catalyst (Fig. 2d) is significantly different, namely less regular than for the alloy catalyst produced by chemical reduction and the catalyst particles are significantly larger, namely in the 1–5  $\mu$ m particle size range. As expected, it is seen that ball-milling introduces a large number of mechanical defects on the catalysts surface, i.e., broken edges, corners, etc.

EDX analysis suggested bulk ratios of 70–30 ( $\pm$ 5) at.% of Pt to Ru for all four Pt/Ru catalysts, thus confirming that the bulk and nominal Pt to Ru ratios are essentially the same for these catalysts. The alloy, thermal and H<sub>2</sub> reduced catalysts consisted of solely Pt and Ru, while the EDX analyses showed that the ball-mill catalyst also contains significant amounts of Al, its composition being: 49:21:30 at.% of Pt:Ru:Al.

### 3.2. Pt surface area conversion factors extracted from combined (COOH)<sub>2</sub> and CO<sub>ads</sub> oxidation studies

It has been shown in previous work that beneficial information about the Pt/Ru catalyst surface can be gained by combining activation controlled (COOH)<sub>2</sub> oxidation currents and CO<sub>ads</sub> oxidation charge measurements [9]. The (COOH)<sub>2</sub> oxidation reaction probes only the Pt surface, and can hence be used to obtain the electro-active Pt area,  $A_{Pt}$ , while CO adsorbs on Pt as well as metallic Ru surface sites [9]. The fact is that the CO<sub>ads</sub> to CO<sub>2</sub> oxidation charge  $Q_{CO_{ads}}$ , in combination with the Pt area estimated using the (COOH)<sub>2</sub> oxidation method, can be used to obtain information of the number of CO molecules adsorbed on catalyst sites other than Pt. This number is reflected in the conversion factor,  $f_{A_{Pt}}$ , that is defined, as follows [9]:

$$f_{A_{Pt}} = \frac{420(\mu\text{C cm}^{-2})}{Q_{CO_{ads}}} \times A_{Pt} \quad (6)$$

Since the Pt surface area,  $A_{Pt}$ , is known from the (COOH)<sub>2</sub> experiments, the anodic charge associated with CO<sub>ads</sub> oxidation at Pt is easily calculated as 420  $\mu\text{C cm}^{-2}$  times  $A_{Pt}$ ; dividing this value by the actual CO<sub>ads</sub> oxidation charge gives the fraction of Pt sites versus the total number of sites, which are active for CO adsorption. In previous work, the  $f_{A_{Pt}}$  factors for the particular catalyst powders studied in this work have been determined and are as follows: Pt powder: 1; PtRu (chemically reduced) powder: 0.7; Pt/RuO<sub>2</sub> (thermal): 0.55; Pt/Ru (H<sub>2</sub> reduced): 0.45 and Pt/RuO<sub>2</sub> (ball-mill): 0.5. It has been shown that the  $f_{A_{Pt}}$  factors present a direct measurement of the fraction of CO adsorbed on Pt sites, and in the case of bi-metallic Pt/Ru catalysts, the value  $(1 - f_{A_{Pt}})$  yields the fraction of CO stripped from metallic Ru sites. A unity value indicates that 100% of the adsorbed CO is stripped from Pt sites, while a  $f_{A_{Pt}}$  factor of 0.7 indicates that 70% of the CO adsorbs on Pt sites and 30% of the CO adsorbs on metallic Ru sites. The  $f_{A_{Pt}}$  factors for the four Pt/Ru catalysts used in this work are less than unity. This indicates that at least some Ru catalyst surface sites are present as Ru metal in the potential range used for the adsorption of CO, i.e., 0.1 V. The data also suggest that the surfaces of all catalysts, except for the PtRu (chemically reduced) powder, are enriched in Ru, i.e., the Pt to Ru surface ratio is higher than the 30 at.% nominal Ru value. This is consistent with the XPS studies. Furthermore, the larger  $f_{A_{Pt}}$  value for the thermal versus the H<sub>2</sub> reduced catalyst suggests that a larger fraction of the surface Ru is present in the metallic state at 0.1 V (where CO is adsorbed) for the latter. This, in turn, indicates that the Ru-oxide present on the surface of the thermal catalyst is not entirely reduced to Ru metal. In fact, the  $f_{A_{Pt}}$  factors for the H<sub>2</sub> reduced and the thermal catalyst suggest that 1.5 times less of the Ru surface sites are in the reduced state at 0.1 V for the latter catalyst. (This involves the plausible assumption that at 0.1 V, all Ru surface sites are in the reduced metallic state for the H<sub>2</sub> reduced catalyst.) The value of 1.5, in turn, suggests that for

the thermal catalyst, ca. 35% of the Ru surface sites are in the oxidized form, which is not active for adsorption of CO at this potential.

### 3.3. Summary of the catalyst properties: bulk and surface characteristics

Based on the results presented above, the Pt/Ru catalysts prepared in this work in their as-prepared states are reviewed and summarized in this section. The PtRu (chemically reduced) catalyst powder appears to consist of a bulk PtRu alloy with a surface consisting of randomly distributed Pt to Ru sites of 70–30 at.% composition, i.e., to have the same bulk and surface compositions (see Section 3.3 for further experimental support). The Pt/Ru (H<sub>2</sub> reduced) catalyst is believed to consist of non-alloyed Pt particles that are coated with Ru islands. The surface is enriched in Ru and the Ru islands consist of mainly Ru metal and easily reducible Ru-oxides. The Pt/RuO<sub>2</sub> (thermal) catalyst is believed to be very similar to the Pt/Ru (H<sub>2</sub> reduced) catalyst. However, the Ru islands of the former mainly consist of RuO<sub>2</sub> and RuO. The exact size and shape of the Ru islands is not known. The Pt/RuO<sub>2</sub> (ball-mill) catalyst also consists of a bulk PtRu alloy of the same composition as the PtRu (chemically reduced catalyst). Its surface, however, is enriched with Ru, i.e., possibly consisting of randomly distributed Pt to Ru sites as well as some Ru islands. The ball-mill catalyst also contains aluminum. Aluminum is expected to not be active for the CO<sub>ads</sub> and CH<sub>3</sub>OH oxidation reactions. In all cases, CO<sub>ads</sub> stripping voltammetry was carried out before and after a set of oxidation experiments. The CO<sub>ads</sub> stripping voltamograms were essentially the same indicating that the catalyst surfaces were not altered during the oxidation experiments.

### 3.4. CO<sub>ads</sub> stripping voltammetry

CO<sub>ads</sub> stripping voltammetry can yield useful in situ electrochemical information about Pt-based catalyst surfaces in the electrochemical environment and has been employed as a probe for the surface composition for PtRu alloys [7]. Fig. 3a–e show typical CO<sub>ads</sub> stripping voltamograms recorded at 10 mV s<sup>-1</sup> for the Pt based powders prepared in this work. The overall CO<sub>ads</sub> stripping charge ( $Q_{CO_{ads}}$ ) estimated for a particular catalyst powder is used to normalize the y-axis ( $i/Q_{CO_{ads}}$ ) in these voltamograms to better compare the data. Table 3 summarizes various characteristics extracted from these voltamograms, namely the onset potential ( $E_{on}$ ) for the CO<sub>ads</sub> to CO<sub>2</sub> oxidation reaction, and the peak width of the CO<sub>ads</sub> stripping peaks measured at peak half height ( $E_{FWHM}$ ). As mentioned above, the CO<sub>ads</sub> stripping voltamogram for the PtRu (chemically reduced) powder used in this work is essentially the same as reported for a sputter cleaned PtRu bulk alloy that is proposed to consist of homogeneously distributed Pt and Ru surface sites at the atomic level of 70–30 at.% Pt to Ru surface composition [18]. This suggests that the very rapid and simultaneous reduction of the

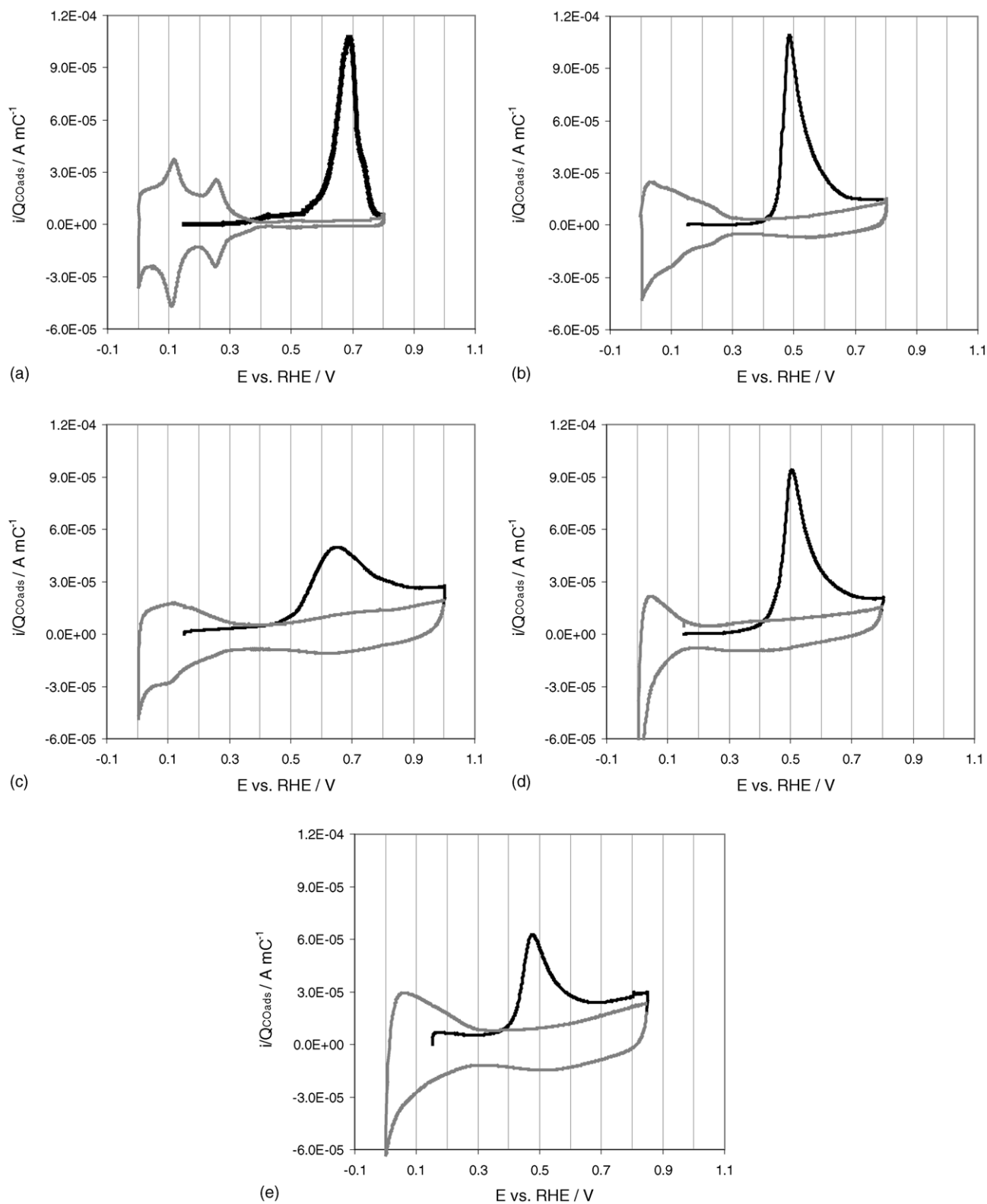


Fig. 3.  $\text{CO}_{\text{ads}}$  stripping voltamograms recorded at  $10 \text{ mV s}^{-1}$  in  $0.5 \text{ M H}_2\text{SO}_4$ . The CO was adsorbed at  $0.1 \text{ V}$  for  $15 \text{ min}$ , subsequently, the solution CO was removed by Argon bubbling for  $30 \text{ min}$  maintaining the potential at  $0.1 \text{ V}$ . The black line shows the first cycle, i.e., the  $\text{CO}_{\text{ads}}$  stripping voltamogram, while the grey line shows the second cycle that is equivalent to the background CV of the particular catalyst powder. (a) The data for the Pt powder, (b) for the PtRu (chemically reduced), (c) for the Pt/RuO<sub>2</sub> (thermal) powder, (d) for the Pt/Ru (H<sub>2</sub> reduced) powder and (e) shows the same for the Pt/RuO<sub>2</sub> (ball-mill) powder. The current axes are normalized using the  $\text{CO}_{\text{ads}}$  charge values extracted from the corresponding  $\text{CO}_{\text{ads}}$  stripping voltamograms.

Table 3  
CO<sub>ads</sub> stripping characteristics<sup>a</sup> for the Pt and Pt/Ru powder catalysts

Catalyst	$E_{\text{on}}$ (V) CO <sub>ads</sub> → CO <sub>2</sub> vs. RHE	$E_{\text{pa}}$ (V) vs. RHE	$E_{\text{FWHM}}$ (mV)
Pt	0.54 <sup>b</sup>	0.69	70 ± 5
PtRu (chemically reduced)	0.42	0.49	80 ± 5
Pt/RuO <sub>2</sub> (thermal)	0.45	0.66	320 ± 20
Pt/Ru (H <sub>2</sub> reduced)	0.43	0.51	110 ± 10
Pt/RuO <sub>2</sub> (ball-mill)	0.39	0.48	100 ± 20

<sup>a</sup> CO<sub>ads</sub> stripping CVs were recorded at 10 mV s<sup>-1</sup> in 0.5 M H<sub>2</sub>SO<sub>4</sub>.

<sup>b</sup> Onset potential ( $E_{\text{on}}$ ) estimated using the larger CO<sub>ads</sub> stripping peak.

Pt- and Ru-precursor salts results in alloyed catalysts consisting of surfaces made of well-distributed Pt to Ru sites [5]. All the Ru containing catalyst powders used in this work exhibit at least a partial bi-functional catalytic effect. This is seen in the lower onset potentials for the CO<sub>ads</sub> oxidation reactions for the four Pt/Ru catalysts in comparison to that observed for the Ru-free Pt powder catalyst. This beneficial effect is assigned to the bi-functional mechanism, i.e., the formation of “Ru–OH” species at low potentials shown in Eqs. (1)–(4). A partial beneficial catalytic effect is also observed for the case for the Pt/RuO<sub>2</sub> (thermal) powder catalyst, although the CO<sub>ads</sub> oxidation peak for this powder is much broader expanding into the more positive potential region than observed for Pt. This indicates that the complete CO<sub>ads</sub> to CO<sub>2</sub> oxidation reaction for this particular catalyst is extremely slow. The lowest onset potential for the CO<sub>ads</sub> to CO<sub>2</sub> oxidation reaction is observed for the Pt/RuO<sub>2</sub> (ball-mill) catalyst and the CO<sub>ads</sub> stripping peak is narrow. A narrow CO<sub>ads</sub> stripping peak and low CO<sub>ads</sub> oxidation potential are also observed for the Pt/Ru (H<sub>2</sub> reduced) catalyst. These results suggest the H<sub>2</sub> reduced catalyst has significantly better oxidation kinetics for the complete CO<sub>ads</sub> to CO<sub>2</sub> oxidation reaction than the Pt/RuO<sub>2</sub> (thermal) catalyst. This significant difference in the

CO<sub>ads</sub> oxidation kinetics is likely due to the different oxidation states of the Ru ad-metal for these otherwise very similar catalysts.

The sweep rate was observed to influence the CO<sub>ads</sub> stripping characteristics for all four Pt/Ru powders. This is seen in Fig. 4a and b that show the dependence of the  $E_{\text{on}}$  and  $E_{\text{FWHM}}$  values on the logarithms of the sweep rate for the four Pt/Ru catalysts. Such a behavior is well known [19] and indicates that the CO<sub>ads</sub> reaction is kinetically limited under the selected experimental conditions. A shift in the  $E_{\text{on}}$  value to more negative potential and a decrease in the  $E_{\text{FWHM}}$  values with decreasing sweep rate are observed for the four Pt/Ru catalysts. Over the entire sweep rate range tested, the lowest  $E_{\text{on}}$  values are observed for the ball-mill catalyst. This indicates that this catalyst has very active and possibly a high number of –OH nucleation sites. The Pt/Ru (H<sub>2</sub> reduced) catalyst is also seen to have low  $E_{\text{on}}$  values that are in fact lower than observed for the PtRu (chemically reduced) catalyst at a particular sweep rate. However, the  $E_{\text{FWHM}}$  values are larger for the H<sub>2</sub> reduced than for the chemically reduced catalyst, indicating that the complete CO<sub>ads</sub> oxidation reaction is slower for the former. This is attributed to the poorer distribution of Pt to Ru surface sites of the H<sub>2</sub> reduced catalyst, which in turn is believed to result in longer CO<sub>ads</sub> diffusion distances. Over the entire sweep rate range studied, the Pt/RuO<sub>2</sub> (thermal) catalyst is seen to clearly exhibit the poorest CO<sub>ads</sub> oxidation kinetics, as reflected in the high  $E_{\text{on}}$  as well as the large  $E_{\text{FWHM}}$  values.

### 3.5. Potentiostatic CO<sub>ads</sub> oxidation: current–time transients

CO<sub>ads</sub> oxidation current-transients recorded at a constant potential provide more detailed information about the CO<sub>ads</sub> oxidation kinetics than CO<sub>ads</sub> stripping CVs. Current–time

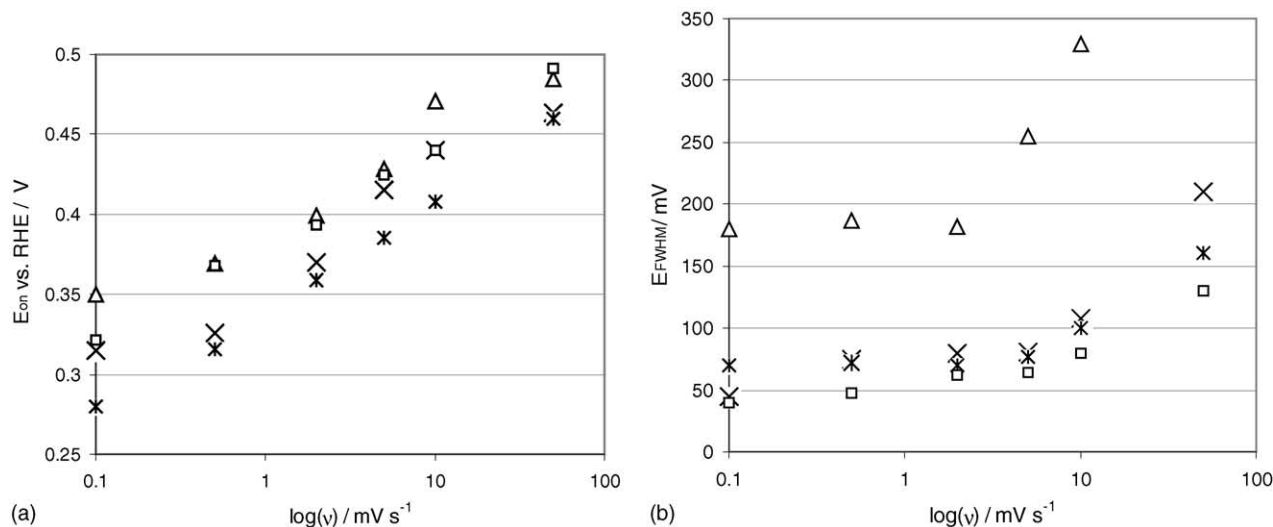


Fig. 4. Dependence of (a) the onset potential ( $E_{\text{on}}$ ) and (b) the  $E_{\text{FWHM}}$  values of the CO<sub>ads</sub> stripping reaction, respectively, on the log of the sweep rate for the Pt/Ru catalysts. (□) shows the data for the PtRu (chemically reduced) catalyst, (Δ) for the Pt/RuO<sub>2</sub> (thermal) catalyst, (×) for the Pt/Ru (H<sub>2</sub> reduced) and (✕) for the Pt/RuO<sub>2</sub> (ball-mill) catalyst. The  $E_{\text{on}}$  values are reported vs. the RHE.

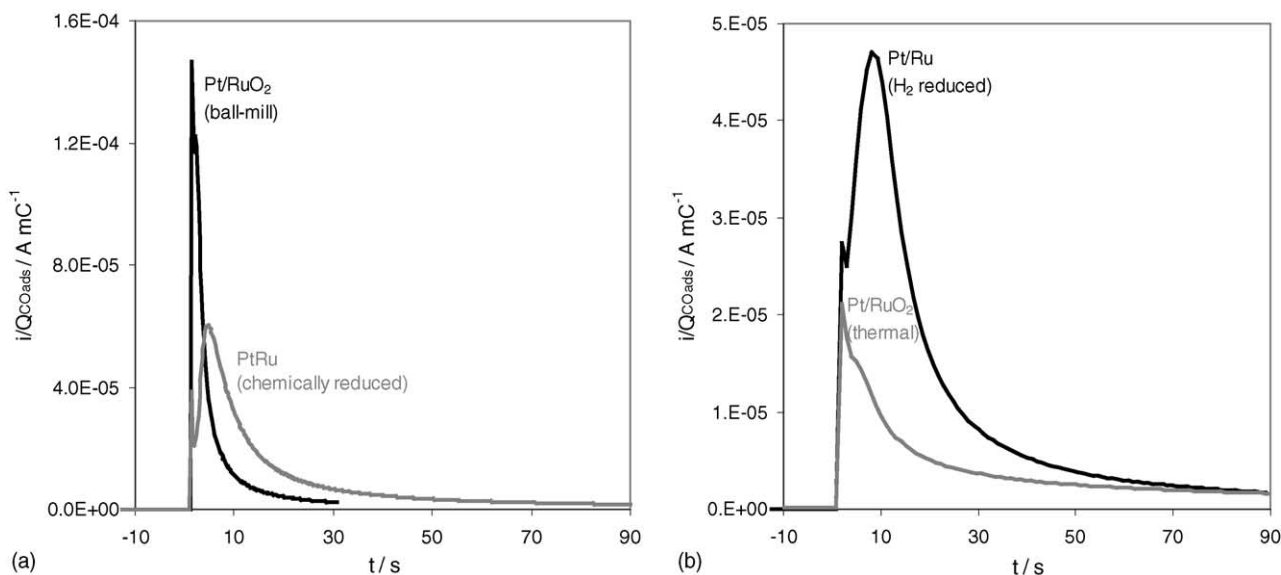


Fig. 5.  $CO_{ads}$  oxidation transients ( $i/Q_{CO_{ads}}$ )– $t$  plots recorded at 0.45 V for (a) the PtRu (chemically reduced) and Pt/RuO<sub>2</sub> ball-mill catalysts and (b) the Pt/Ru(H<sub>2</sub> reduced) and Pt/RuO<sub>2</sub> (thermal) catalysts. The current axes are normalized using the  $CO_{ads}$  charge extracted from the corresponding  $CO_{ads}$  stripping voltamograms.

transients for the  $CO_{ads}$  oxidation reaction for Pt/Ru systems have been reported previously in the literature [19,20]. In the following sections, experimentally observed current–time transients recorded at two particular potentials will be discussed. In this work, low potentials are selected at which the Pt–OH formation reaction can be ignored, i.e., only Ru sites are believed to serve as –OH nucleation sites. Subsequently, the data will be analyzed to obtain information about the –OH nucleation rate and the surface diffusion of CO. Experimental  $CO_{ads}$  oxidation current–time ( $i/Q_{CO_{ads}}$ )– $t$  transients are shown in Fig. 5a and b. The ( $i/Q_{CO_{ads}}$ )– $t$  transients were recorded at 0.45 V and the currents are normalized using the  $Q_{CO_{ads}}$  values extracted from the corresponding CV data. Under these conditions, the  $CO_{ads}$  reaction is seen to be the most rapid using the Pt/RuO<sub>2</sub> (ball-mill) catalyst, followed by the PtRu (chemically reduced), the Pt/Ru (H<sub>2</sub> reduced) and finally the Pt/RuO<sub>2</sub> (thermal) catalyst. The initial high current rise seen in these transients is due to double layer charging. This was confirmed by ( $i/Q_{CO_{ads}}$ )– $t$  transients recorded in the absence of CO, i.e., in the H<sub>2</sub>SO<sub>4</sub> background solution. The asymmetrical, i.e., tailing current decay indicates that CO surface diffusion to –OH nucleation sites is rate determining in the  $CO_{ads}$  to  $CO_2$  oxidation reaction [20]. Such a tailing current is observed for all four catalysts indicating that  $CO_{ads}$  surface diffusion plays a significant role in the  $CO_{ads}$  to  $CO_2$  oxidation reaction for all four Pt/Ru catalyst systems studied here. A similar tailing current of comparable time scale to the PtRu (chemically reduced) catalyst has been reported in previous work for catalysts of “proposed” homogeneously distributed, at the atomic scale, Pt/Ru surface sites of 70 and 30 at.% composition [19]. This further emphasizes the similarity of the previously studied system [20] and the chemically reduced PtRu catalyst used in this work.

At 0.45 V, complete oxidation of all the CO molecules adsorbed on the catalyst surfaces was found to take ca. 30 s for the Pt/RuO<sub>2</sub> (ball-mill) catalyst, ca. 70 and 90 s for the PtRu (chemically reduced) and Pt/Ru (H<sub>2</sub> reduced) catalysts, respectively, and more than 30 min for the Pt/RuO<sub>2</sub> (thermal) catalyst. These data can be used to obtain an estimate for the maximal surface diffusion distance of CO, defined as  $x$ , using the square root approximation [21]:

$$x = \sqrt{Dt} \quad (7)$$

In Eq. (7),  $t$  is the time and  $D$  the CO surface diffusion coefficient. A  $D$  value of  $4 \times 10^{-14} \text{ cm}^2 \text{ s}^{-1}$  is used here that was estimated in previous work based on experimental  $CO_{ads}$  oxidation data for Pt/Ru catalysts [22]. The 30 s needed for the complete oxidation of  $CO_{ads}$  using the Pt/RuO<sub>2</sub> (ball-mill) catalyst suggest that the maximal CO surface diffusion distance on this catalyst surface is ca. 11 nm. This is equivalent to ca. 40 Pt atoms using a lattice constant of 0.3 nm. The same calculations for the other three Pt/Ru catalysts suggest a maximal CO surface diffusion distance of ca. 20 nm, equivalent to ca. 65 Pt atoms for the PtRu (chemically reduced) and the Pt/Ru (H<sub>2</sub> reduced) catalysts and more than 90 nm, i.e., more than 300 Pt atoms for the Pt/RuO<sub>2</sub> (thermal) catalyst. These are significant CO surface diffusion distances for all catalysts, in particular for the ball-mill and chemically reduced catalysts considering that they presumably consist of surfaces with homogeneously distributed Pt and Ru sites. In the case of a catalyst surface that truly consists of atomic level, homogeneously distributed Pt to Ru sites of 70–30 at.% composition, each Pt sites is located next to a Ru site. Therefore, diffusion of  $CO_{ads}$  to a Ru site is not needed if all Ru sites are equally active as –OH nucleation sites. The suggested surface diffusion of CO over as many as 40 and 65 Pt

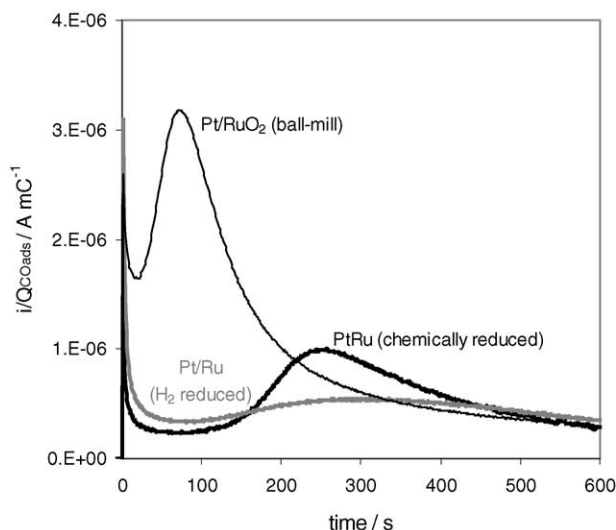


Fig. 6.  $\text{CO}_{\text{ads}}$  oxidation transients  $(i/Q_{\text{CO}_{\text{ads}}})-t$  plots recorded at 0.35 V for the PtRu (chemically reduced), the Pt/Ru( $\text{H}_2$  reduced) and the Pt/Ru $\text{O}_2$  (ball-mill) catalyst. The currents are normalized using the corresponding  $\text{CO}_{\text{ads}}$  charge ( $Q_{\text{CO}_{\text{ads}}}$ ) extracted from the  $\text{CO}_{\text{ads}}$  stripping voltamogram data recorded at  $10 \text{ mV s}^{-1}$ .

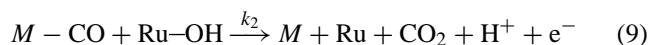
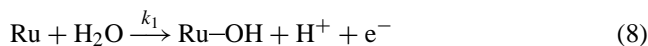
atoms for the two catalysts (that are believed to be made up of surfaces of well-distributed Pt and Ru sites) suggests that not all Ru sites are equally active for the  $\text{CO}_{\text{ads}}$  oxidation and the  $-\text{OH}$  formation reaction. This is not unexpected considering the fact that Ru is well known to show a range of energetically different surface sites towards its oxidation reaction [23]. Indeed, this results in the close to ideal super-capacitive behavior of Ru and Ru-oxides [23].

An interesting difference is seen in the  $(i/Q_{\text{CO}_{\text{ads}}})-t$  transients between the PtRu (chemically reduced) and the Pt/Ru ( $\text{H}_2$  reduced) catalysts for short versus longer times of anodic polarization. During the initial few seconds, the  $\text{CO}_{\text{ads}}$  oxidation currents for the chemically reduced catalyst are higher than for the  $\text{H}_2$  reduced catalyst indicating a faster reaction. This is clearly seen in  $(i/Q_{\text{CO}_{\text{ads}}})-t$  transients recorded at 0.35 V that are shown in Fig. 6 for the ball-mill, chemically reduced and  $\text{H}_2$  reduced catalysts. At this low potential, an “induction” period (late raise and low magnitude of the oxidation current) is observed, which is seen to be most pronounced for the chemically reduced catalyst. In fact, the  $\text{H}_2$  reduced catalyst shows a higher  $\text{CO}_{\text{ads}}$  oxidation current at shorter times (during the initial ca. 100 s), while the rate is lower (compared with the chemically reduced catalyst) at longer times. This suggests that the  $\text{H}_2$  reduced catalyst has a few  $-\text{OH}$  nucleation sites that are more active than the chemically reduced catalyst, which is consistent with the low  $E_{\text{on}}$  values observed in the  $\text{CO}_{\text{ads}}$  stripping voltamograms. The initially more rapid formation of  $-\text{OH}$  nucleation sites for the  $\text{H}_2$  reduced catalyst, as compared to the chemically reduced catalyst, may be linked to the fact that the former has “large” Ru-islands on its surface. The current intensity of the Pt/Ru $\text{O}_2$  (thermal) catalyst at 0.35 V is too low to observe a maximum and complete removal of  $\text{CO}_{\text{ads}}$  at this potential

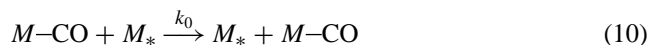
takes longer than 1 h. Therefore, the  $(i/Q_{\text{CO}_{\text{ads}}})-t$  transient for this catalyst is not shown in Fig. 6. The double layer charging and the  $\text{CO}_{\text{ads}}$  oxidation currents are clearly separated in the transients recorded at 0.35 V. At this low potential, the majority of the Ru sites are believed to be in the reduced state, i.e., Ru is in the metallic state for the ball-mill, chemically reduced and the  $\text{H}_2$  reduced catalysts [9]. For both the chemically reduced and  $\text{H}_2$  reduced catalysts, the 10 min at 0.35 V used to record the transients shown in Fig. 6 are insufficient to oxidize all of the  $\text{CO}_{\text{ads}}$  molecules. This was confirmed by subsequent  $\text{CO}_{\text{ads}}$  stripping voltammetry that indicated that during the 10 min at 0.35 V, 59 and 32% of the  $\text{CO}_{\text{ads}}$  were oxidized in the case of the chemically reduced and the  $\text{H}_2$  reduced catalysts, respectively. The fact that a larger number of  $\text{CO}_{\text{ads}}$  molecules are oxidized for the chemically reduced than for the  $\text{H}_2$  reduced catalyst in the 10 min at 0.35 V suggests again that the  $\text{CO}_{\text{ads}}$  oxidation reaction is overall faster for the chemically reduced than the poorly distributed Pt to Ru surface sites of the  $\text{H}_2$  reduced catalyst.

### 3.6. Analysis of the $(i/Q_{\text{CO}_{\text{ads}}})-t$ transients: rate of $-\text{OH}$ nucleation site formation

The  $\text{CO}_{\text{ads}}$  oxidation reaction is viewed to take place according to the bi-functional mechanism as follows [2]:



In Eq. (9),  $M$  is either a Ru or Pt surface site. According to this scheme, “ $\text{CO}_{\text{ads}}$ -free” Ru sites need to be present to form  $\text{Ru}-\text{OH}$ . This is of particular importance for surfaces with high  $\text{CO}_{\text{ads}}$  coverage. As the  $\text{CO}_{\text{ads}}$  oxidation reaction proceeds, an increasingly higher number of Ru sites are freed from adsorbed CO and become potential  $-\text{OH}$  nucleation sites. This results in an increase in the oxidation current, which in fact is clearly observed in the experimental  $(i/Q_{\text{CO}_{\text{ads}}})-t$  transients. In order to oxidize  $\text{CO}_{\text{ads}}$  to  $\text{CO}_2$ , the  $\text{CO}_{\text{ads}}$  must be located close to a  $-\text{OH}$  nucleation site. At a high  $\text{CO}_{\text{ads}}$  coverage and relatively low number of  $-\text{OH}$  nucleation sites, a large number of adsorbed CO molecules are located in close vicinity to a nucleation site. However, as the  $\text{CO}_{\text{ads}}$  oxidation reaction proceeds, and if no new  $-\text{OH}$  nucleation sites are generated, CO needs to first diffuse across the catalyst surface to be subsequently oxidized to  $\text{CO}_2$ . This  $\text{CO}_{\text{ads}}$  surface diffusion process involves free catalyst surface sites,  $M_*$ , i.e.,



Therefore, the complete  $\text{CO}_{\text{ads}}$  to  $\text{CO}_2$  oxidation reaction can be described as follows: initially, cylindrical CO concentration profiles develop around active  $-\text{OH}$  nucleation sites. The individual diffusion profiles eventually overlap and rather complicated  $\text{CO}_{\text{ads}}$  diffusion profiles can develop depending on the Pt to Ru surface site distribution. If the

diffusion of surface adsorbed CO to a –OH nucleation site is rate determining in the CO<sub>ads</sub> to CO<sub>2</sub> oxidation reaction, and if no new or a very small number of new –OH nucleation sites are formed, a decrease in the oxidation current is observed. This suggests that the increase in the oxidation current in the  $i/(Q_{\text{CO}_{\text{ads}}})-t$  transients represents a measure of the sum of the formation rate and number of –OH nucleation sites as well as the oxidation rate of CO adsorbed on sites in direct contact with an active –OH nucleation site.

Such a CO<sub>ads</sub> oxidation mechanism suggests that the CO<sub>ads</sub> oxidation transients can be used to extract several valuable characteristic numbers. The initial rising slope of the current–transient,  $d(i/Q_{\text{CO}_{\text{ads}}})/dt$ , represents the rate of the “–OH nucleation” site formation and oxidation of nearby CO<sub>ads</sub> species. The time needed to reach the current maxima,  $t_0$ , represents the period when –OH nucleation sites are formed at a measurable rate. The charge passed to reach this maximum,  $Q_0$ , represents a measurement of the number of –OH nucleation sites. It should be noted that the oxidation of CO molecules located on nearby sites also contributes to the  $Q_0$  values. Therefore, the percentage of the  $Q_0$  per total  $Q_{\text{CO}_{\text{ads}}}$  value, i.e., the  $Q_0$  (%) value reflects the number of –OH nucleation sites formed and the number of CO<sub>ads</sub> molecules in close vicinity to such sites, and can be used to compare different catalysts. One characteristic of a good CO<sub>ads</sub> to CO<sub>2</sub> oxidation catalyst is its capability to form a high number of –OH nucleation sites and oxidize a large number of CO<sub>ads</sub> molecules within a short time period. This is reflected in a large  $Q_0$  (%) /  $t_0$  ratio. Values for  $t_0$ ,  $Q_0$  (%) and  $Q_0$  (%) /  $t_0$  are summarized in Table 4. The values are extracted from the  $(i/Q_{\text{CO}_{\text{ads}}})-t$  transients at 0.45 and 0.35 V for the four Pt/Ru catalyst powders studied in this work. The  $Q_0$  (%) /  $t_0$  values are seen to decay in the following order at both potentials: Pt/RuO<sub>2</sub> (ball-mill)  $\gg$  PtRu (chemically reduced)  $>$  Pt/Ru (H<sub>2</sub> reduced)  $\gg$  Pt/RuO<sub>2</sub> (thermal). This order represents the capability of a catalyst to form –OH nucleation sites and oxidize CO<sub>ads</sub> molecules, i.e., suggesting that the ball-mill catalyst is superior to the chemically and H<sub>2</sub> reduced catalysts, and that the thermal catalyst has a very poor capability to form –OH nucleation sites. In fact, the  $(i/Q_{\text{CO}_{\text{ads}}})-t$  transients recorded at 0.35 V for the thermal catalyst did not show a current maxima and the oxidation charge measured during this period of 10 min was very small, thus indicating a very poor capability of this catalyst to produce –OH nucleation sites at this potential. The PtRu (chemically reduced) catalyst appears to display only a slightly better ac-

tivity for the CO<sub>ads</sub> oxidation reaction than the H<sub>2</sub> reduced catalyst despite its better Pt to Ru surface site distribution. This adds further support to the view that the Ru sites are not equally active as –OH nucleation sites. The origin of the better CO<sub>ads</sub> oxidation kinetics for the ball-mill versus the chemically reduced catalyst is not yet clear. In both cases, the Pt to Ru surface sites are believed to be well distributed and bulk PtRu alloys of similar compositions are formed. The better CO<sub>ads</sub> oxidation kinetics, which are clearly linked to a more rapid –OH nucleation rate for the ball-mill versus the chemically reduced catalyst, may be linked to the fact that the Ru surface concentration of the ball-mill catalyst is higher. Furthermore, ball-milling introduces mechanical stress and the morphology of these two catalysts will be significantly different. Therefore, a possibly higher number of surface defect sites may be at least partly responsible for the observed improved CO<sub>ads</sub> oxidation kinetics of the ball-mill catalyst.

It should be noted that electronic effects introduced by alloying Pt and Ru can also influence the CO<sub>ads</sub> oxidation kinetics. According to ab-initio calculations, alloying of Pt with Ru weakens the Ru–CO bond in the 0.1 eV range, while increasing the concentration of Ru in the alloy lattice is proposed to weaken the Pt–CO bond substantially; differences of up to 0.5 eV have been reported [24]. The fact that we observe experimentally that the oxidation reaction of the CO molecules adsorbed on presumably the Ru sites takes place on the same time scale for the PtRu alloy and the two phase Pt and Ru islands, i.e., the Pt/Ru (H<sub>2</sub> reduced catalyst) could indicate that the electronic influence of alloying on the Ru–CO bond has a smaller effect than predicted by ab-initio calculations that involve a number of assumptions. Statements regarding the influence of electronic effects of alloying on the strength of Pt–CO bond cannot be made using the catalysts systems prepared and experiments carried out in this work.

### 3.7. CH<sub>3</sub>OH oxidation studies

Fig. 7 shows Tafel plots, i.e., the potential ( $E$ ) versus the logarithms of the CH<sub>3</sub>OH oxidation current normalized for the electro-active Pt area ( $j_{\text{CH}_3\text{OH}}$ ), obtained at 20 °C for the Pt and Pt/Ru powder catalysts studied in this work. The CH<sub>3</sub>OH oxidation currents were obtained from current–time transients recorded at a particular potential. In all cases, a decay of the oxidation current was observed that approached a pseudo steady-state value after several minutes. The CH<sub>3</sub>OH oxidation current values used for the plots

Table 4  
Characteristic numbers for the CO<sub>ads</sub> oxidation reaction carried out at a particular potential for Pt/Ru catalysts

Catalyst	$t_0$ (s <sup>-1</sup> ) at 0.45 V	$Q_0$ (%) at 0.45 V	$Q_0/t_0$ (% s <sup>-1</sup> ) at 0.45 V	$t_0$ (s <sup>-1</sup> ) at 0.35 V	$Q_0$ (%) at 0.35 V	$Q_0/t_0$ (% s <sup>-1</sup> ) at 0.35 V
PtRu (chemically reduced)	5.5	13	2.4	260	11	0.04
Pt/RuO <sub>2</sub> (thermal)	5	3.5	0.7	n.a. <sup>a</sup>	n.a. <sup>a</sup>	n.a. <sup>a</sup>
Pt/Ru (H <sub>2</sub> reduced)	8	17	2.1	300	10	0.03
Pt/RuO <sub>2</sub> (ball-mill)	1.2	10	8.3	80	14	0.2

Ratio vs. the corresponding  $t_0$  value found for the ball-mill catalyst.

<sup>a</sup> No maxima observed.

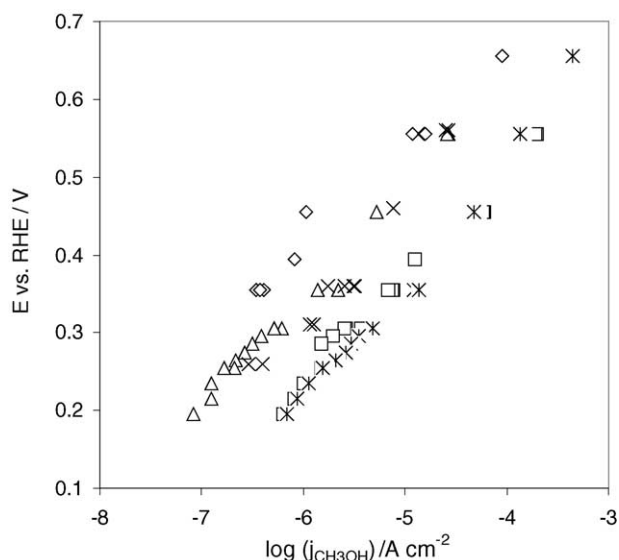


Fig. 7.  $\text{CH}_3\text{OH}$  oxidation current ( $j_{\text{CH}_3\text{OH}}$ )–potential ( $E$ ) curves for ( $\diamond$ ) Pt, ( $\square$ ), PtRu (chemically reduced), ( $\times$ ) Pt/RuO<sub>2</sub> (ball-mill), ( $*$ ) Pt/Ru (H<sub>2</sub> reduced) and ( $\triangle$ ) Pt/RuO<sub>2</sub> (thermal) catalysts. The  $\text{CH}_3\text{OH}$  oxidation currents are pseudo-steady state values that were extracted after applying a particular potential for 20 min.

shown in Fig. 7 were extracted from the pseudo steady-state values, i.e., 20 min after applying a particular potential. Prior to the recording of each  $\text{CH}_3\text{OH}$  oxidation current–time transients, the potential was held at 0.1 V for 30 s. This allowed the recording of reproducible current–time transients, as discussed in detail elsewhere [5]. The amount of catalyst deposited on the Au substrate was adjusted depending on the potential range and catalyst investigated. In all cases, electrodes were prepared that resulted in  $\text{CH}_3\text{OH}$  oxidation currents of less than 10 mA. At such low currents, minimal amounts of H<sub>2</sub> are produced at the counter electrode, and hence a possible interference of this with the anode reaction can be ruled out.

The dependence of the  $\text{CH}_3\text{OH}$  oxidation current on the potential is essentially the same for the four Pt/Ru catalysts. For all four Pt/Ru powder catalysts, two regions with Tafel slopes of a ca. 120 mV per  $\log(j_{\text{CH}_3\text{OH}})$  and an anomalous slope of ca. 200 mV per  $\log(j_{\text{CH}_3\text{OH}})$  are observed. The Tafel slopes of ca. 120 mV per  $\log(j_{\text{CH}_3\text{OH}})$  are observed at lower potentials and indicate that an initial one electron electrochemical reaction is rate determining in the  $\text{CH}_3\text{OH}$  oxidation reaction. At these low potentials, the  $-\text{OH}$  formation reaction on Ru sites (i.e., Eq. (3)) is generally viewed to be rate determining which is consistent with a 120 mV per  $\log(j_{\text{CH}_3\text{OH}})$  Tafel slope. The origin of the anomalous, larger than 120 mV per  $\log(j_{\text{CH}_3\text{OH}})$  slope is not understood and beyond the scope of this work. It is, however, in agreement with previously reported values [25]. In Fig. 7, the  $\text{CH}_3\text{OH}$  oxidation currents are normalized for the Pt area using the  $f_{\text{A}_{\text{Pt}}}$  factors as discussed in a previous section of this work. Therefore, the  $\text{CH}_3\text{OH}$  oxidation data shown in Fig. 7 represent true catalytic activities. It is seen that the  $\text{CH}_3\text{OH}$  oxidation activity for the chemically reduced and ball-mill catalysts are

essentially the same. They are ca. seven times higher than the  $\text{CH}_3\text{OH}$  oxidation activity for the H<sub>2</sub> reduced and the thermal catalysts over the entire potential range investigated in this work. The activity of the H<sub>2</sub> reduced and thermal catalysts are essentially the same. The activity of the ball-mill and the chemically reduced catalysts are ca. 30 times higher than for the Pt catalyst, which is in good agreement with literature data that showed a ca. 30 times increase in catalytic activity for sputter-cleaned bulk PtRu alloy catalysts of 70–30 at.% Pt to Ru composition over polycrystalline platinum [5]. Fig. 7 shows that all four Pt/Ru catalysts show better  $\text{CH}_3\text{OH}$  oxidation activities than the Pt powder, thus indicating that all four Pt/Ru catalysts exhibit a beneficial catalytic effect as also seen for the  $\text{CO}_{\text{ads}}$  oxidation reaction. However, the type of Pt/Ru catalyst is seen to influence the  $\text{CH}_3\text{OH}$  and  $\text{CO}_{\text{ads}}$  oxidation reactions differently. In fact, the  $\text{CH}_3\text{OH}$  oxidation activities can be placed in two groups; namely, essentially the same activity for the ball-mill and chemically reduced catalysts and essentially the same activity for the H<sub>2</sub> reduced and thermal catalysts. The clearly better  $\text{CH}_3\text{OH}$  oxidation activity for the ball-mill and chemically reduced catalysts over the H<sub>2</sub> reduced and thermal catalysts is suggested to be due to the better distribution of Pt to Ru sites on the surface of the first two catalysts in the present work. In fact, it appears that the  $\text{CH}_3\text{OH}$  activity is determined by the optimal number of Pt and nearby Ru sites that is clearly better for catalysts that are alloyed and consist of surfaces made of well-distributed Pt to Ru sites rather than the oxidation state of the Ru ad-metal of the as-prepared catalyst. It should be noted that in this work, the catalytic activities are compared to the Ru ad-metal state of the as-prepared catalysts and cannot be correlated to the most active ad-metal state of Ru during the reaction. It is very well possible that Ru-oxides of these Pt/Ru catalysts are at least partially reduced to Ru metal in the electrochemical environment, as has been indeed shown in previous work [8,9].

#### 4. Summary and conclusions

A range of unsupported Pt/Ru catalyst powders of the same nominal Pt to Ru ratios of 70–30 at.% were prepared and characterized. A PtRu alloy powder catalyst that is viewed to be of homogenous composition and the same bulk and surface Pt and Ru concentration was made via a very rapid chemical reduction method. Two non-homogenous Pt/Ru powders were made that consist of a non-alloyed Pt phase and a surface enriched with Ru. The first powder was made by thermally decomposing RuCl<sub>3</sub> on Pt powder and is referred to as thermal catalyst. Part of this powder was then reduced in a H<sub>2</sub> atmosphere resulting in the second non-homogenous Pt/Ru powder referred to as H<sub>2</sub> reduced catalyst. The form of the Ru ad-metal of these two as-prepared catalysts is different, i.e., RuO<sub>2</sub> and lower, easily reducible lower Ru-oxides for the thermal catalyst powder, and mainly Ru metal and easily reducible lower Ru-oxides for the H<sub>2</sub> reduced catalyst powder. A Pt/Ru powder catalyst

was also prepared by ball-milling Pt and RuO<sub>2</sub> resulting in a bulk PtRu alloy that appears, however, to be surface enriched in Ru. The surface Ru was found to be present as Ru metal and lower, easily reducible Ru-oxides.

The catalysts were used to study the CO<sub>ads</sub> and CH<sub>3</sub>OH oxidation reactions. Their catalytic activities were compared to the properties of the as-prepared catalysts. The CO<sub>ads</sub> oxidation reaction was studied in a potential range where the contribution of –OH formation on Pt sites can be assumed to be very small. It has been shown that several characteristics can be extracted from CO<sub>ads</sub> oxidation experiments that allow the comparison of these complex catalyst systems with regard to –OH nucleation rates and Pt to Ru site distributions. It was found that there is no direct correlation between the capabilities of these catalysts to oxidize CO<sub>ads</sub> and CH<sub>3</sub>OH. In the case of the CO<sub>ads</sub> oxidation reaction, the presence of RuO<sub>2</sub> in combination with poorly distributed Pt to Ru sites on the catalyst surface was found to result in a significantly slower CO<sub>ads</sub> oxidation reaction. The formation of active –OH species on the Ru sites are needed for the CO<sub>ads</sub> to CO<sub>2</sub> oxidation reaction according to the bi-functional mechanism, Eqs. (8) and (9) was very low for the catalyst containing RuO<sub>2</sub> on its surface. The presence of Ru in the metallic state on the as-prepared catalyst surface clearly resulted in faster CO<sub>ads</sub> oxidation reaction kinetics and higher –OH nucleation rates. The fastest CO<sub>ads</sub> oxidation kinetics were found for catalysts made of well-distributed Pt to Ru surface sites. This is attributed to the smaller surface diffusion distances needed for the CO to diffuse to an active –OH nucleation site on these catalyst surfaces consisting of well-distributed Pt to Ru sites. For all catalysts, asymmetrical CO<sub>ads</sub> oxidation current–time transients were observed indicating that surface diffusion of CO to an –OH nucleation site is rate determining. The maximal CO<sub>ads</sub> diffusion lengths were estimated and long CO<sub>ads</sub> diffusion distances were found, even for the catalyst surfaces consisting of well-distributed Pt to Ru sites. The major factor determining the CH<sub>3</sub>OH oxidation activity was found to be the Pt to Ru surface site distribution. Highest CH<sub>3</sub>OH oxidation activities were found for the Pt/Ru catalysts that consisted of well-distributed Pt to Ru surface sites, while the oxidation state of the Ru ad-metal of the as-prepared catalyst appears not to influence the catalytic CH<sub>3</sub>OH oxidation activity. This suggests that an optimal arrangement of Pt and nearby Ru sites is essential for the CH<sub>3</sub>OH oxidation reaction rather than the Ru surface state of the as-prepared catalysts. The observed kinetic differences for these catalysts to oxidize CO<sub>ads</sub> and CH<sub>3</sub>OH may be partly related to the fact that in the former case, CO is adsorbed on both Pt and Ru sites, while CH<sub>3</sub>OH adsorbs from solution onto Pt sites only.

## Acknowledgements

The authors thank G. Pleizier and D. Kingston (NRC, Ottawa) for the XPS analysis and J. Margeson (NRC, Ottawa) for the FESEM and EDX analyses as well as P. L'Abbe (NRC, Ottawa) for the preparation of the electrochemical glass cells used in this work. Financial support from the NRC fuel cell program is also greatly acknowledged.

## References

- [1] J.O'M. Bockris, H. Wroblowa, *J. Electroanal. Chem.* 7 (1964) 428.
- [2] M. Watanabe, S. Motoo, *J. Electroanal. Chem.* 60 (1975) 267.
- [3] H. Gasteiger, N. Markovic, P. Ross, E. Cairns, *J. Electrochem. Soc.* 141 (1994) 1795.
- [4] H. Hoster, T. Iwasita, H. Baumgartner, W. Vielstich, *Phys. Chem. Chem. Phys.* 3 (2001) 337.
- [5] C. Bock, B. MacDougall, Y. LePage, *J. Electrochem. Soc.* 151 (2004) A1269.
- [6] J.W. Long, R.M. Stroud, K.E. Swider-Lyons, D.R. Rolison, *J. Phys. Chem. B* 104 (2000) 9772.
- [7] H.N. Dinh, X. Ren, F.H. Garzon, P. Zelenay, S. Gottesfeld, *J. Electroanal. Chem.* 491 (2000) 222.
- [8] H. Kim, I.R. deMoraes, G. Tremiliosi, R. Haasch, A. Wieckowski, *Surf. Sci.* 474 (2001) L203.
- [9] C. Bock, B. MacDougall, *J. Electrochem. Soc.* 150 (2003) 377.
- [10] K. Lasch, L. Joerisson, K.A. Friedrich, J. Garche, *J. Solid State Electrochem.* 7 (2003) 619.
- [11] A.H.C. Sirk, J.M. Hill, S.K.Y. Kung, V.I. Birss, *J. Phys. Chem. B* 108 (2004) 689.
- [12] M.C. Denis, P. Guerec, D. Guay, J.P. Dodelet, G. Lalande, R. Schulz, *J. Appl. Electrochem.* 30 (2000) 1243.
- [13] A.J. Bard, L.R. Faulkner, *Electrochemical Methods, Fundamentals and Applications*, John Wiley & Sons, 1980.
- [14] X-ray Diffraction Database, Diffraction Management System for Windows NT, Scintag Inc., Cupertino, California (1997).
- [15] L.X. Yang, C. Bock, B. MacDougall, J. Park, *J. Appl. Electrochem.* 34 (2004) 427.
- [16] G. Lalande, M.C. Denis, P. Guerec, D. Guay, J.P. Dodelet, R. Schulz, *J. New Mater. Electrochem. Syst.* 3 (2000) 185.
- [17] T.A.F. Lassali, J.F.C. Boodts, S.C. DeCastro, R. Landers, S. Trasatti, *Electrochim. Acta* 39 (1994) 95.
- [18] H.A. Gasteiger, P.N. Ross, E.J. Cairns, *J. Surf. Sci.* 293 (1993) 67.
- [19] H.A. Gasteiger, N. Markovic, P.N. Ross, E.J. Cairns, *J. Phys. Chem.* 98 (1994) 617.
- [20] F. Maillard, M. Eikerling, O.V. Cherstiouk, S. Schreier, E. Savinova, U. Stimming, *Faraday Discuss.* 125 (2004) 357.
- [21] J.O'M. Bockris, A.K.N. Reddy, *Modern Electrochemistry*, vol. 1, A Plenum/Rosetta ed., Plenum Press, New York, 1970.
- [22] K.A. Friedrich, K.P. Geysers, A. Marmann, U. Stimming, R. Vogel, *Zeitschrift fuer Physikalische Chemie* 208 (1999) 137.
- [23] S. Hadzi-Jordanov, H. Angerstein-Kozłowska, B.E. Conway, *J. Electroanal. Chem.* 60 (1975) 359.
- [24] T.E. Shubina, M.T.M. Koper, *Electrochim. Acta* 47 (2002) 3621.
- [25] W. Chrzanowski, A. Wieckowski, *Langmuir* 14 (1998).